PNAS RESEARCH ARTICLE | CELL BIOLOGY

ATOH8 binds SMAD3 to induce cellular senescence and prevent Ras-driven malignant transformation

Ximeng Liu[a,1], Xu Li[a,1], Shuang Wang[a,1], Qin Liu[a], Xianming Feng[a], Wenting Wang[a], Zhangduo Huang[b], Yongbo Huang[c], Jueheng Wu[a], Muyan Cai[d], Xiuyu Cai[e], Xiaonan Xu[f], Junchao Cai[a,g,2], and Mengfeng Li[b,2]

Edited by Anton Berns, Antoni van Leeuwenhoek Nederlands Kanker Instituut, Amsterdam, Netherlands; received June 12, 2022; accepted October 13, 2022

The process of oncogene-induced senescence (OIS) and the conversion between OIS and malignant transformation during carcinogenesis is poorly understood. Here, we show that following overactivation of oncogene Ras in lung epithelial cells, high-level transforming growth factor β1 (TGF-β1)–activated SMAD3, but not SMAD2 or SMAD4, plays a determinant role in inducing cellular senescence independent of the p53/p16/p15 senescence pathways. Importantly, SMAD3 binds a potential tumor suppressor ATOH8 to form a transcriptional complex that directly represses a series of cell cycle–promoting genes and consequently causes senescence in lung epithelial cells. Interestingly, the prosenescent SMAD3 converts to being oncogenic and essentially facilitates oncogenic Ras-driven malignant transformation. Furthermore, depleting Atoh8 rapidly accelerates oncogenic Ras-driven lung tumorigenesis, and lung cancers driven by mutant Ras and Atoh8 loss, but not by mutant Ras only, are sensitive to treatment of a specific SMAD3 inhibitor. Moreover, hypermethylation of the *ATOH8* gene can be found in approximately 12% of clinical lung cancer cases. Together, our findings demonstrate not only epithelial cellular senescence directed by a potential tumor suppressor–controlled transcriptional program but also an important interplay between the prosenescent and transforming effects of TGF-β/SMAD3, potentially laying a foundation for developing early detection and anticancer strategies.

cellular senescence | malignant transformation | TGF-β | SMAD3 | Ras

Oncogene overactivation due to genetic mutation is a common driving force for malignant transformation of a normal cell to be a cancer cell, such as Kirsten rat sarcoma (KRas) mutation (1, 2). Ectopic expression of mutant Ras in cultured normal cells, however, induces a permanent and irreversible growth arrest known as oncogene-induced senescence (OIS) (3, 4). OIS is broadly recognized as an intrinsic defense against malignant transformation and is characterized by senescence-associated secretory phenotype (SASP) and permanent growth arrest, for which the p38/p16 and p53/p21 proteins have been identified as crucial promoters (5, 6). Nevertheless, overexpression of these promoters alone or together can markedly slow cell growth but is usually insufficient to cause the senescent phenotype. SASP, which consists of various cytokines, growth factors, and proteolytic enzymes, can play both tumor-suppressive and tumor-promoting roles (7). Whether and how the double-edge SASP participates in the conversion from OIS to malignant transformation remains largely uncovered.

As a critical SASP component, transforming growth factor-β1 (TGF-β1) alone is sufficient to induce senescence in various cell types (8, 9). The cytostatic effects during TGF-β–induced cellular senescence are largely mediated by cell cycle regulators, such as induction of p15, p21, and p27 or suppression of c-myc and hTERT (8, 10–12). Moreover, TGF-β signaling is involved in Ultra Violet (UV) exposure- and oxidative stress–induced cellular senescence (13, 14). Interestingly, TGF-β family ligands also play a notable role in the SASP-induced paracrine senescence of neighboring normal cells (9, 15). Tumor-associated macrophages secrete TGF-β1 as a critical inducer of cellular senescence to limit Myc-driven lymphomagenesis (16). By contrast, TGF-β is also well known for its function as a tumor promoter via inducing epithelial–mesenchymal transition (EMT), augmenting tumor metastasis, and predisposing an immune-suppressive tumor microenvironment (17). Yet, how TGF-β manipulates its prosenescent tumor-suppressive functions and switches to oncogenic roles during tumor development needs further investigation.

The TGF-β signaling relies on the SMAD protein family containing eight members (18). Following TGF-β stimulation, their serine kinase receptors are phosphorylated to activate SMAD2 and SMAD3, which usually form homo- or heterotrimer with SMAD4 to regulate downstream target gene expression. Transcription of selected target genes, and the biological consequence of the TGF-β signaling, is strongly determined by contextual

Significance

How normal cells escape oncogene-induced senescence (OIS) and become malignant tumor cells remains largely unclear. Herein, we report that p53/p16/p15-independent senescence, which is mediated by TGF-β1–induced SMAD3–ATOH8–directed anti–cell cycle transcriptional program, is a barrier to oncogenic Ras-driven tumorigenesis in lung epithelial cells. ATOH8 loss switches the prosenescent effect of TGF-β1/SMAD3 to be oncogenic, facilitates transformation of lung epithelial cells to become lung cancer cells, and accelerates Ras-driven lung tumorigenesis in a manner requiring SMAD3. The potential tumor suppressor ATOH8 is inactivated by aberrant hypermethylation in lung cancer. Altogether, our study displays an important interplay between the prosenescent and transforming effects of TGF-β/SMAD3 underlying mutant Ras–driven senescence and oncogenesis.

Author contributions: J.C. and M.L. designed research; X. Liu, X. Li, S.W., Q.L., X.F., W.W., Z.H., and X.X. performed research; Y.H., J.W., M.C., and X.C. contributed new reagents/analytic tools; and X. Liu, J.C. and M.L. wrote the paper.

The authors declare no competing interest.

This article is a PNAS Direct Submission.

[1]X. Liu, X. Li, and S.W. contributed equally to this work.

[2]To whom correspondence may be addressed. Email: caijch3@mail.sysu.edu.cn or limf@mail.sysu.edu.cn.

This article contains supporting information online at https://www.pnas.org/lookup/suppl/doi:10.1073/pnas.2208927120/-/DCSupplemental.

Published January 10, 2023.

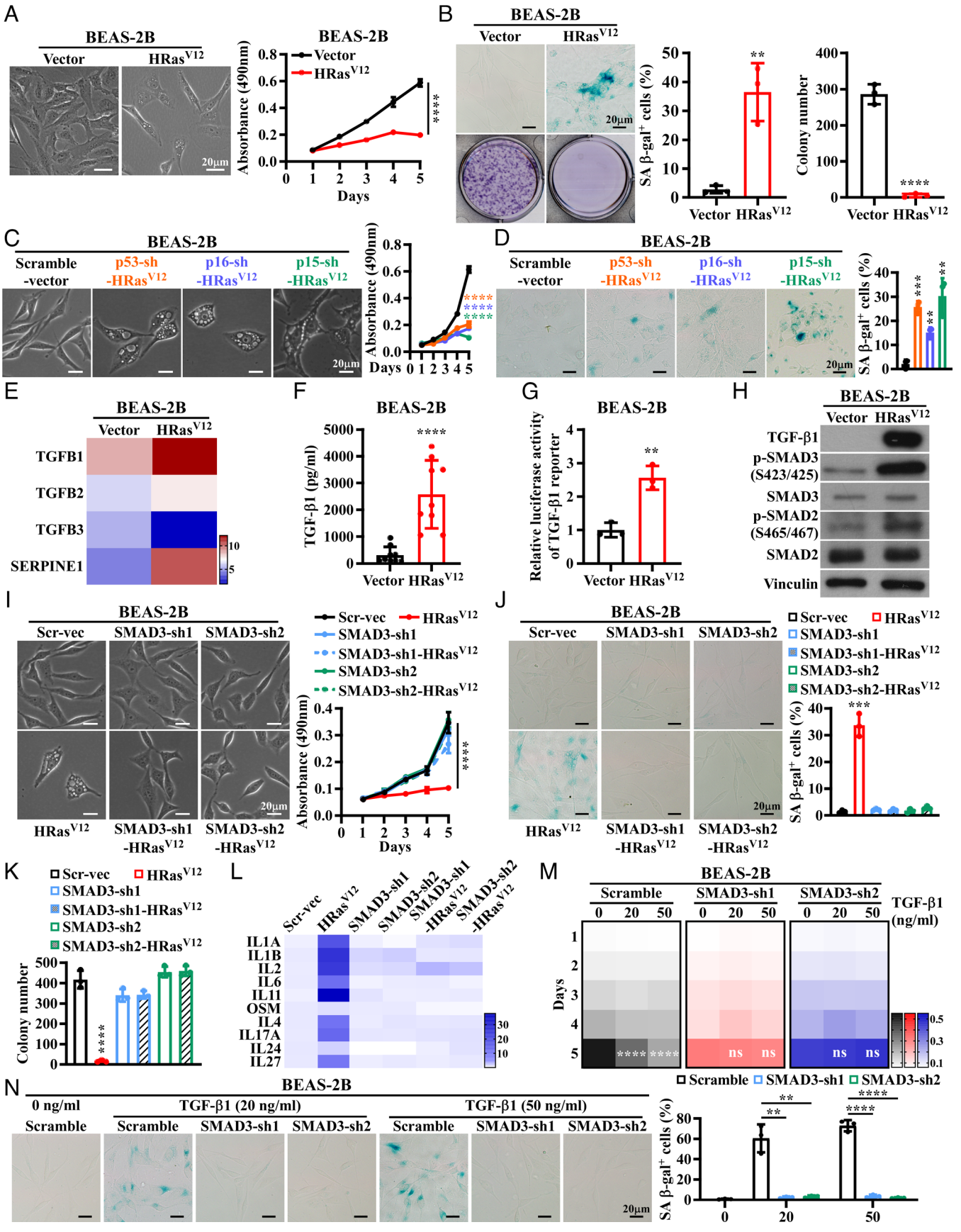

Fig. 1. The TGF-β1/SMAD3 pathway importantly contributes to RIS. (*A*) Representative morphology images and Methyl Thiazolyl Tetrazolium (MTT) assay of BEAS-2B cells that stably overexpressed HRas^{V12} or control vectors. (*B*) Representative images and quantification of SA-β-gal–positive cells or cell colonies. (*C* and *D*) Representative cellular morphology, cell proliferation, and analysis of SA-β-gal–positive cells are shown. (*E*) Heat map shows the top dysregulated genes in the TGF-β signaling induced by HRas^{V12}. (*F*) Enzyme-linked Immunosorbent Assay (ELISA) analysis of TGF-β1 concentration in culture medium of indicated cells. (*G*) The effect of overexpressing HRas^{V12} on TGF-β1 transcriptional activity. (*H*) Western blot (WB) detection of indicated proteins. (*I–K*) Representative morphology

factors such as receptor type, the form of SMAD complex, and transcriptional cofactors (18, 19). For example, our previous study showed that SMAD3 and SMAD2 not only co-occupy a series of common target genes but also have distinct profiles of target genes, leading to completely opposite effects on tumor progression (20). Of note, SMAD4 essentially promotes TGF-β–treated premalignant or malignant pancreatic cells to undergo EMT-linked apoptosis, and SMAD4 loss accelerates mutant Ras–driven tumorigenesis, which importantly explains the fact that SMAD4 inactivation occurs in nearly half of pancreatic ductal adenocarcinomas (PDAs) (21). While the roles of SMAD proteins in both the pro- and antitumorigenic effects of TGF-β are soundly described (22, 23), how the SMAD proteins are destined to mediate prosenescent or transforming effects of TGF-β at the early stage of tumor initiation remains unclear.

In this current study, we found that in lung epithelial cells, a potential tumor suppressor ATOH8 binds SMAD3 to directly repress a series of cell cycle–promoting genes, causing cell cycle arrest and essentially contributing to oncogenic Ras- or TGF-β1–induced cellular senescence independent of the p53/p16/p15 pathways. ATOH8 loss switches the prosenescent tumor-suppressive SMAD3 to be oncogenic and converts oncogenic Ras-induced senescence (RIS) into malignant transformation, providing new insights in the process of oncogenic Ras- or TGF-β–mediated cellular senescence and malignant transformation in epithelial cells.

Results

SMAD3 Is Required for Oncogenic Ras- or TGF-β–Induced Cellular Senescence. To investigate the process of OIS and tumorigenesis, we transduced activated HRas ($HRas^{V12}$) into an immortalized bronchial cell line BEAS-2B, whose p53 and p16/Rb pathways are impaired by the SV40 large T antigen, and primarily cultured normal lung epithelial (NLE) cells derived from cancer-adjacent normal lung tissue without p53/p16/Rb loss or Ras mutation to establish oncogenic RIS cell models, which are featured by enlarged and bubble-shaped cell morphology, arrested cell cycle, and strong staining of senescence-associated β-galactosidase (SA-β-gal) (Fig. 1 *A* and *B* and *SI Appendix*, Fig. S1 *A* and *B*). Impressively, not only was the expression of cellular senescence hallmarks p53 and p16, or of a crucial cytostatic effector p15, not altered but also activities of the p53 and p16/Rb pathways remained unchanged in the two RIS models (*SI Appendix*, Fig. S1*C*). Moreover, silencing p53, p16, or p15 failed to resist RIS (Fig. 1 *C* and *D* and *SI Appendix*, Fig. S1*D*). By contrast, TGF-β1 expression, SMAD2 and SMAD3 phosphorylation levels, and TGF-β1 reporter activity were significantly increased in RIS cells (Fig. 1 *E*–*H*). Interestingly, silencing SMAD3, but not SMAD2 or SMAD4, prevented the RIS phenotypes (Fig. 1 *I*–*K* and *SI Appendix*, Fig. S1 *E*–*L*). Of note, silencing SMAD3, but not SMAD2 or SMAD4, markedly abolished expression of a canonical transcriptional target, namely, PAI-1 of the TGF-β signaling, whereas oncogenic Ras still significantly increased SMAD3 phosphorylation and PAI-1 expression in senescent BEAS-2B cells presilenced for SMAD2 or SMAD4 but not in those cells presilenced for SMAD3 (*SI Appendix*, Fig. S1 *E* and *F*). Consistently, silencing SMAD3 markedly abrogated oncogenic Ras-induced expression of numerous SASP molecules (7, 24–27) (Fig. 1*L*). Furthermore, continuous stimulation for 5 d with high concentration (20 or 50 ng/mL) of recombinant TGF-β1 proteins, which are much higher than the physiological concentration of TGF-β1, caused significantly slow growth and induced strong SA-β-gal activity in BEAS-2B cells; notably, low-dose recombinant TGF-β1 (2.5, 5, or 10 ng/mL) failed to induce senescent phenotype in lung epithelial cells, for which we speculate that high-level TGF-β1 might compensate for the effects of many other cytokines. Similarly, silencing SMAD3, rather than SMAD2 or SMAD4, almost completely abrogated TGF-β1–induced growth arrest and senescent phenotypes (Fig. 1 *M* and *N* and *SI Appendix*, Fig. S2 *A* and *B*). Intriguingly, unlike the tumor-suppressive effects of TGF-β through EMT as reported (21), morphological EMT changes of RIS cells were not apparent, and it appears that EMT change is not indispensable for the abovementioned epithelial cellular senescence (*SI Appendix*, Figs. S1 *E* and *F* and S2 *C* and *D*). These data demonstrate that SMAD3, but not SMAD2 or SMAD4, is required for oncogenic Ras- or TGF-β–induced cellular senescence.

ATOH8 Specifically Binds SMAD3 to Form a Transcriptional Complex. We then investigated why SMAD3, but not SMAD2, is required for TGF-β–mediated cellular senescence. Following mass spectrometry analysis, ATOH8 emerged as a strong, specific SMAD3-interactive transcription factor (Fig. 2*A*). Indeed, SMAD3, but not SMAD2 or SMAD4, could directly bind ATOH8 with high affinity, especially in the nucleus of RIS cells (Fig. 2 *B*–*E* and *SI Appendix*, Fig. S3 *A*–*C*). The proline-rich region (PRR) domain of the ATOH8 protein was essential for its binding capacity to the linker domain of SMAD3 (*SI Appendix*, Fig. S3 *D*–*F*). Of note, overexpressing ATOH8 did not interfere the interaction of SMAD3 with SMAD2 or with SMAD4 (Fig. 2*F*). Interestingly, based on ChIP-seq data of SMAD3 and ATOH8 using optimized parameter for peak calling with *P* value of 0.0065, SMAD3 and ATOH8 co-occupied 1,104 target genes, and the proportions of their distribution within genomic regions were highly identical (Fig. 2 *G*–*I*). Moreover, several de novo motifs were identified in both ATOH8- and SMAD3-occupied peaks (Fig. 2*J*). Electrophoretic Mobility Shift Assay (EMSA) verified that ATOH8 could bind chemically synthesized oligonucleotide probes containing a consensus SMAD3-binding motif sequence or the de novo ATOH8- and SMAD3-occupied motif sequence, and silencing SMAD3 markedly diminished the binding of ATOH8 to the oligonucleotide probes (Fig. 2*K*). Consistently, overexpression of only SMAD3-interactive ATOH8 markedly activated the TGF-β signaling pathway (*SI Appendix*, Fig. S3*G*). These data suggest that ATOH8 interacts with SMAD3 to form a unique transcriptional complex and thus significantly contributes to the activation of SMAD3-directed TGF-β signaling pathway.

ATOH8–SMAD3 Transcriptional Complex Induces an Anti–Cell Cycle Signature. Among 1,920 genes repressed and 827 genes induced by ATOH8 overexpression, 122 down-regulated and

images and MTT assay of indicated cells and representative images and quantification of SA-β-gal–positive cells or cell colonies. Scr-vec denotes scramble-vector. (*L*) Expression of SASP genes detected by qRT–PCR. (*M*) MTT assay of indicated BEAS-2B cells treated with 0, 20, or 50 ng/mL TGF-β1 for 5 d. (*N*) Representative images and quantification of SA-β-gal–positive cells following TGF-β1 treatment for 5 d. The SA-β-gal staining, colony formation, and ELISAs were performed at day 5 after stable cell line establishment during (*B, D, F, J*, and *K*) or after continuous TGF-β1 treatment for 5 d (*M* and *N*). Error bars represent mean ± SD derived from at least three or four independent experiments. Two-tailed Student's *t* tests were used for statistical analyses in *B*, *D*, *F*, *G*, *J*, *K*, and *N*. Two-way ANOVA was used for statistical analyses in *A*, *C*, *I*, and *M*. $^{**}P < 0.01$, $^{***}P < 0.001$, $^{****}P < 0.0001$, ns, not significant.

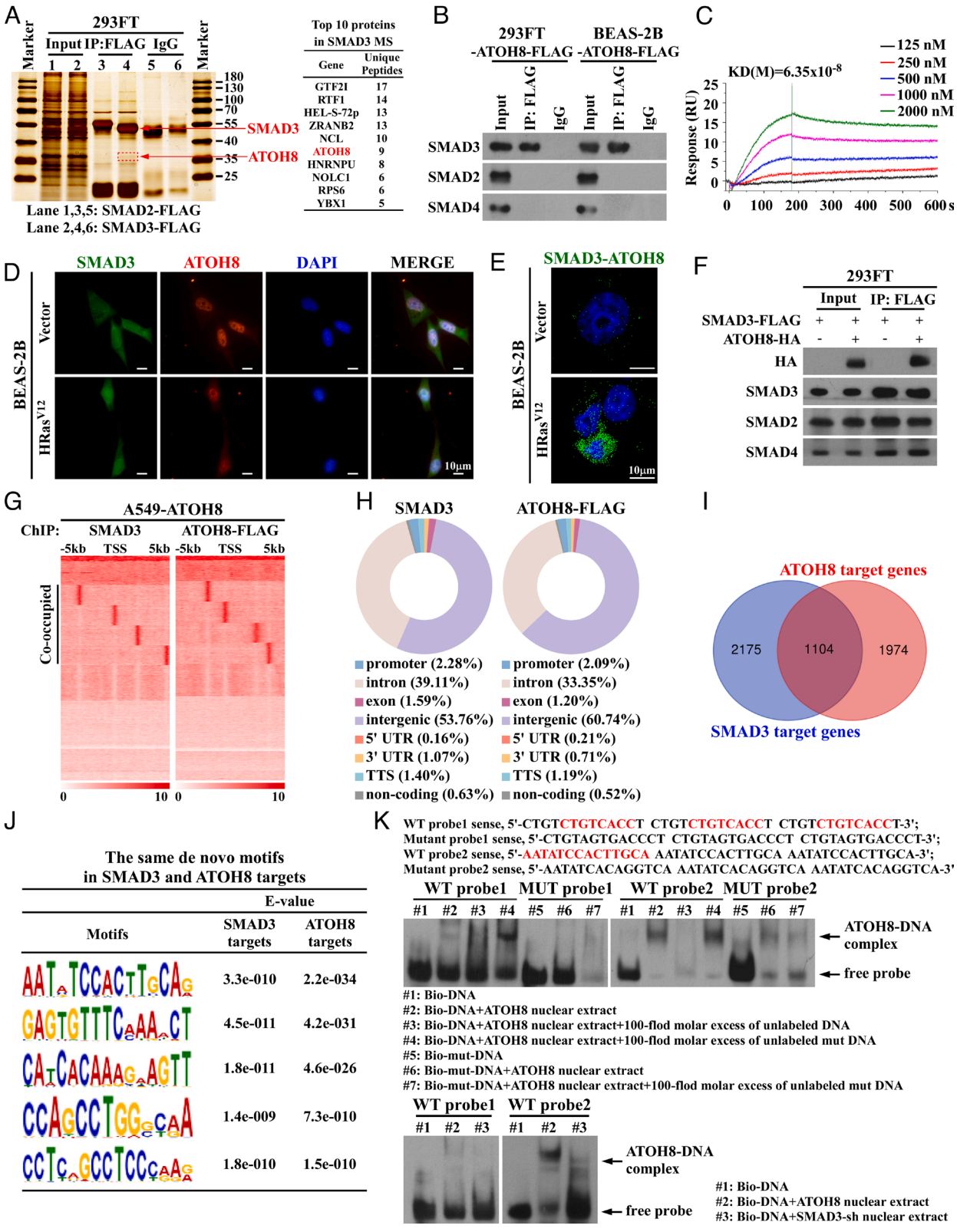

Fig. 2. SMAD3 binds ATOH8 to form a unique transcriptional complex. (*A*) Immunoprecipitated fractions using anti-FLAG affinity purification from lysates of 293FT cells transfected with FLAG-SMAD2 or FLAG-SMAD3 were subjected to mass spectrometry analysis. (*B*) Coimmunoprecipitation analysis of the interaction between indicated proteins. (*C*) Surface Plasmon (SPR) analysis measured the affinity and kinetics of the ATOH8–SMAD3 interaction. (*D* and *E*) Representative images of coimmunostaining of SMAD3 (green) and ATOH8 (red) and Proximity Ligation Assay (PLA) puncta formed by SMAD3–ATOH8 interaction. (*F*) Coimmunoprecipitation assay in 293FT cells when cotransfecting SMAD3 with or without ATOH8. (*G*) Heat map showed the read density for SMAD3- or ATOH8-bound peaks from the ChIP-seq analysis in A549 cells overexpressing FLAG-ATOH8. (*H* and *I*) The genomic annotation and the number of overlapped genes of SMAD3- or ATOH8-bound peaks. (*J*) De novo motif enrichment analysis of SMAD3- or ATOH8-bound peaks. (*K*) Binding between ATOH8 and chemically synthesized oligonucleotide probes as indicated was determined by EMSA.

42 up-regulated genes were identified as ATOH8 and SMAD3 co-occupied transcripts (Fig. 3 *A* and *B* and *SI Appendix*, Fig. S4*A*). The most enriched annotations for the 122 down-regulated target genes were related to cell cycle progression, and ATOH8 expression indeed negatively correlated with their expression (Fig. 3 *C*–*F* and *SI Appendix*, Fig. S4*B*). Among

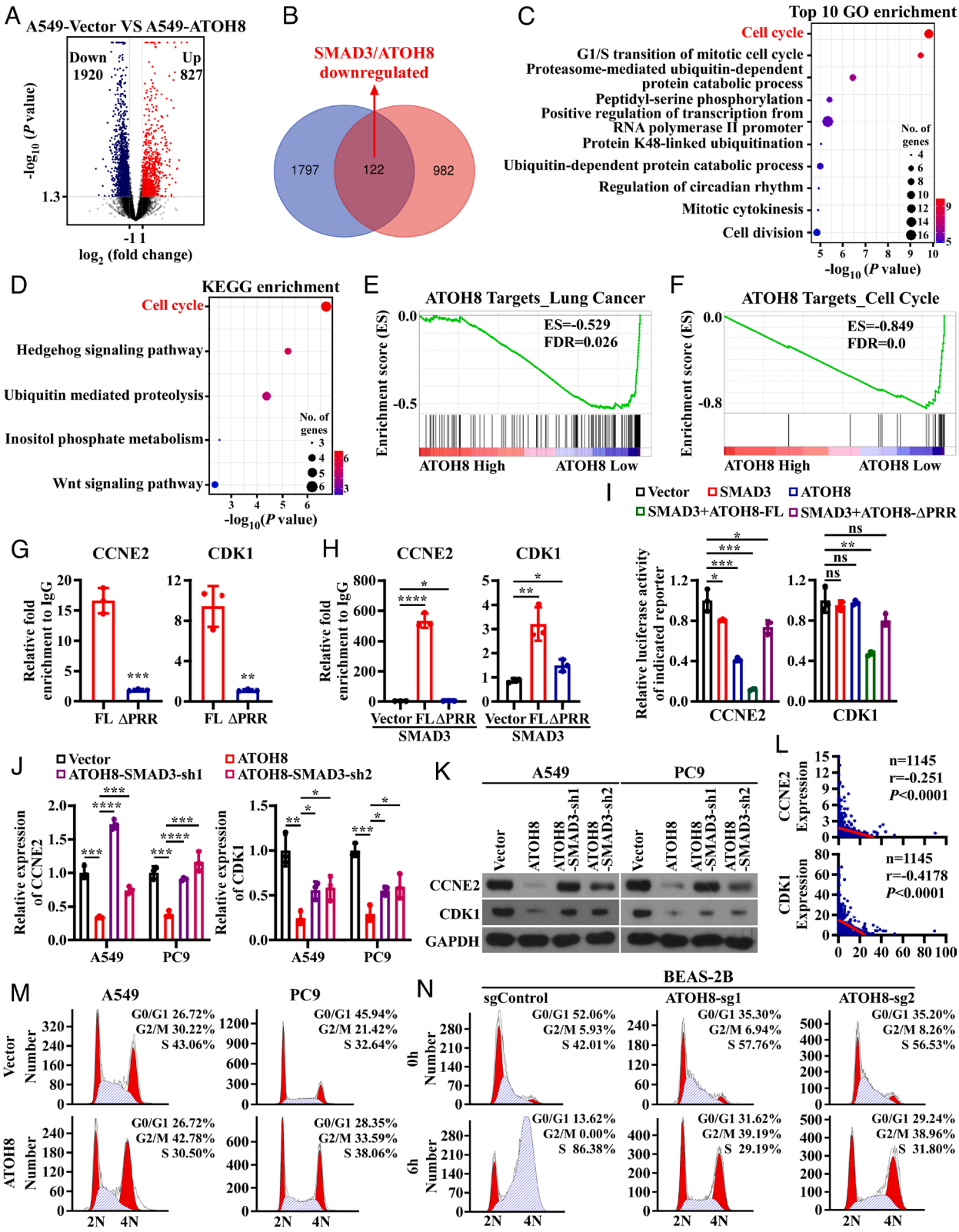

Fig. 3. SMAD3 interacts with ATOH8 to induce an anti–cell cycle program. (*A*) Volcano heat map showed differential expression genes between vector control and ATOH8-overexpressing A549 cells. (*B*) The number of overlapped genes between ATOH8–SMAD3-occupied and ATOH8-down-regulated genes. (*C* and *D*) Gene Ontology (GO) and Kyoto Encyclopedia of Genes and Genomes (KEGG) analysis of the 122 overlapped target genes. (*E* and *F*) Gene Set Enrichment Analysis (GSEA) of the correlation between ATOH8 and 122 down-regulated target genes and 23 cell cycle–promoting genes using the TCGA lung cancer database. (*G–I*) ChIP–qPCR and dual-luciferase reporter assays validated the binding of full-length ATOH8 (FL), ATOH8-△PRR or SMAD3 to *CCNE2* and *CDK1* genes. (*J* and *K*) The effect of ATOH8 overexpression together with SMAD3 silencing on CCNE2 and CDK1 expression. (*L*) Correlation analysis of ATOH8 and CCNE2 or CDK1 expression in the TCGA lung cancer database. (*M* and *N*) Flow cytometric analysis of cell cycle distribution phases of indicated cells was performed after being released from the synchronized G2/M phase for 2 h (*M*) or synchronized G1/S phase for 6 h (*N*). Error bars represent mean ± SD derived from three independent experiments. Two-tailed Student's *t* test was used for statistical analysis in *G*, *H*, *I*, and *J*. *$P < 0.05$, **$P < 0.01$, ***$P < 0.001$, ****$P < 0.0001$, ns, not significant.

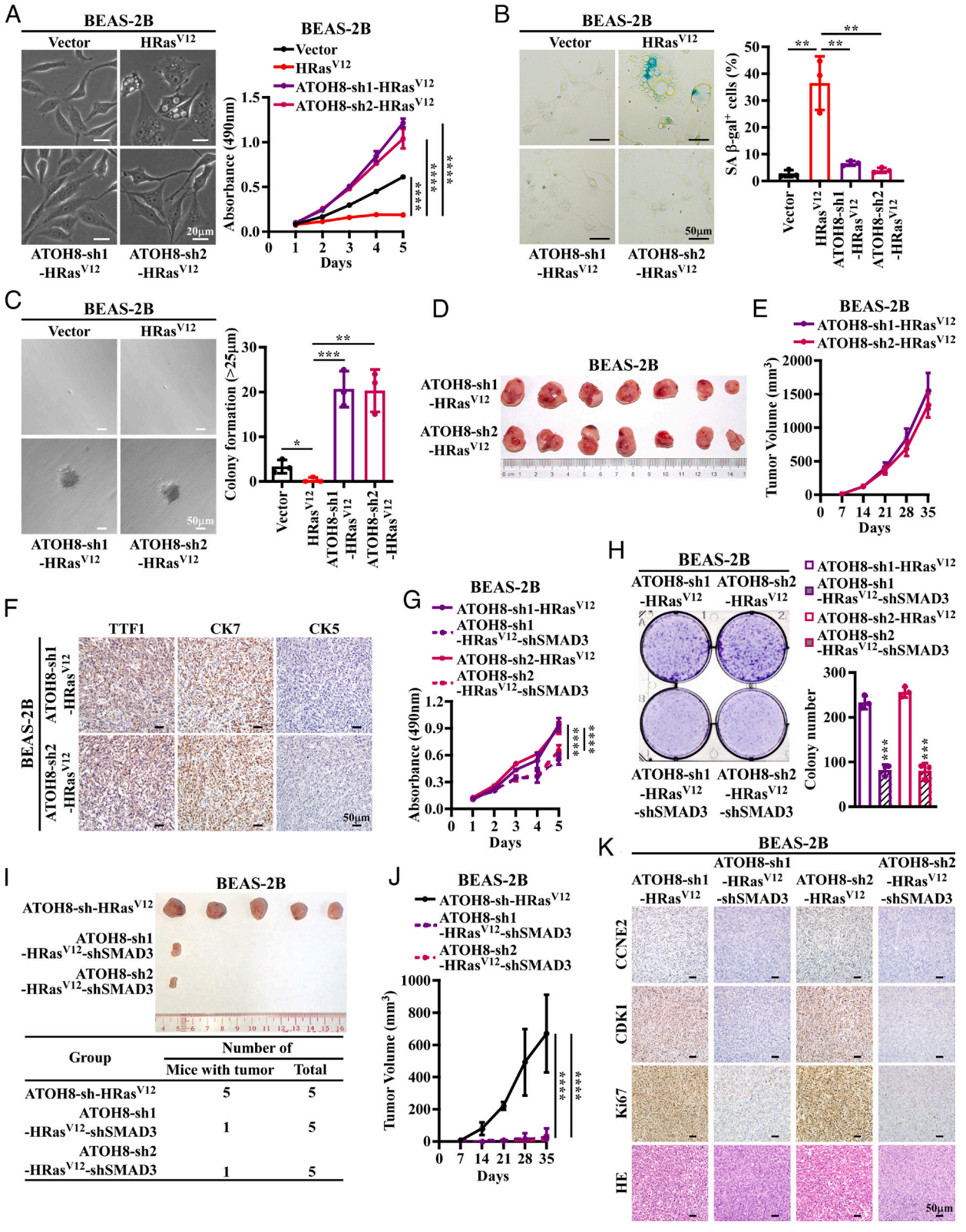

Group	Number of	
	Mice with tumor	Total
ATOH8-sh-HRas^{V12}	5	5
ATOH8-sh1 -HRas^{V12}-shSMAD3	1	5
ATOH8-sh2 -HRas^{V12}-shSMAD3	1	5

Fig. 4. Silencing ATOH8 converts RIS to malignant transformation. (*A*) Representative morphology images and MTT assay of indicated cells. (*B* and *C*) Representative images and quantification of SA-β-gal–positive cells or cell colonies. (*D* and *E*) Excised tumors and growth curves of indicated tumor xenografts (n=7 mice per group). (*F*) Representative images of TTF1, CK7, and CK5 immunostaining of indicated tumor xenografts. (*G* and *H*) The effect of silencing SMAD3 on growth of indicated cells. (*I* and *J*) Excised tumors and growth curves of indicated xenografts (n=5 mice per group). (*K*) Representative images of CCNE2, CDK1, and Ki67 immunostaining and H&E of indicated tumor xenografts. SA-β-gal staining and soft agar assays were performed at day 5 after stable cell line establishment (*B*, *C*, and *H*). Error bars represent mean ± SD derived from three or four independent experiments. Two-tailed Student's *t* test was used for statistical analysis in *B, C,* and *H*. Two-way ANOVA was used for statistical analysis in *A*, *E*, *G*, and *J*. **P* < 0.05, ***P* < 0.01, ****P* < 0.001, and *****P* < 0.0001.

them, the ATOH8–SMAD3 co-occupied promoter/enhancer sequences of CCNE2 and CDK1, which are crucial for the G1/S and G2/M checkpoints, could be immunoprecipitated only by SMAD3-interactive ATOH8 (Fig. 3*G*). In addition, SMAD3 could strongly bind to these sequences in the presence of SMAD3-interactive ATOH8 (Fig. 3*H*), and SMAD3 and

ATOH8 co-overexpression significantly repressed the luciferase expression of reporters containing sequences of CCNE2 or CDK1 gene promoter/enhancer (Fig. 3*I*). As expected, ATOH8 overexpression suppressed CCNE2 and CDK1 expression in a manner requiring SMAD3 (Fig. 3 *J* and *K*). The Cancer Genome Atlas (TCGA) lung cancer datasets also showed a

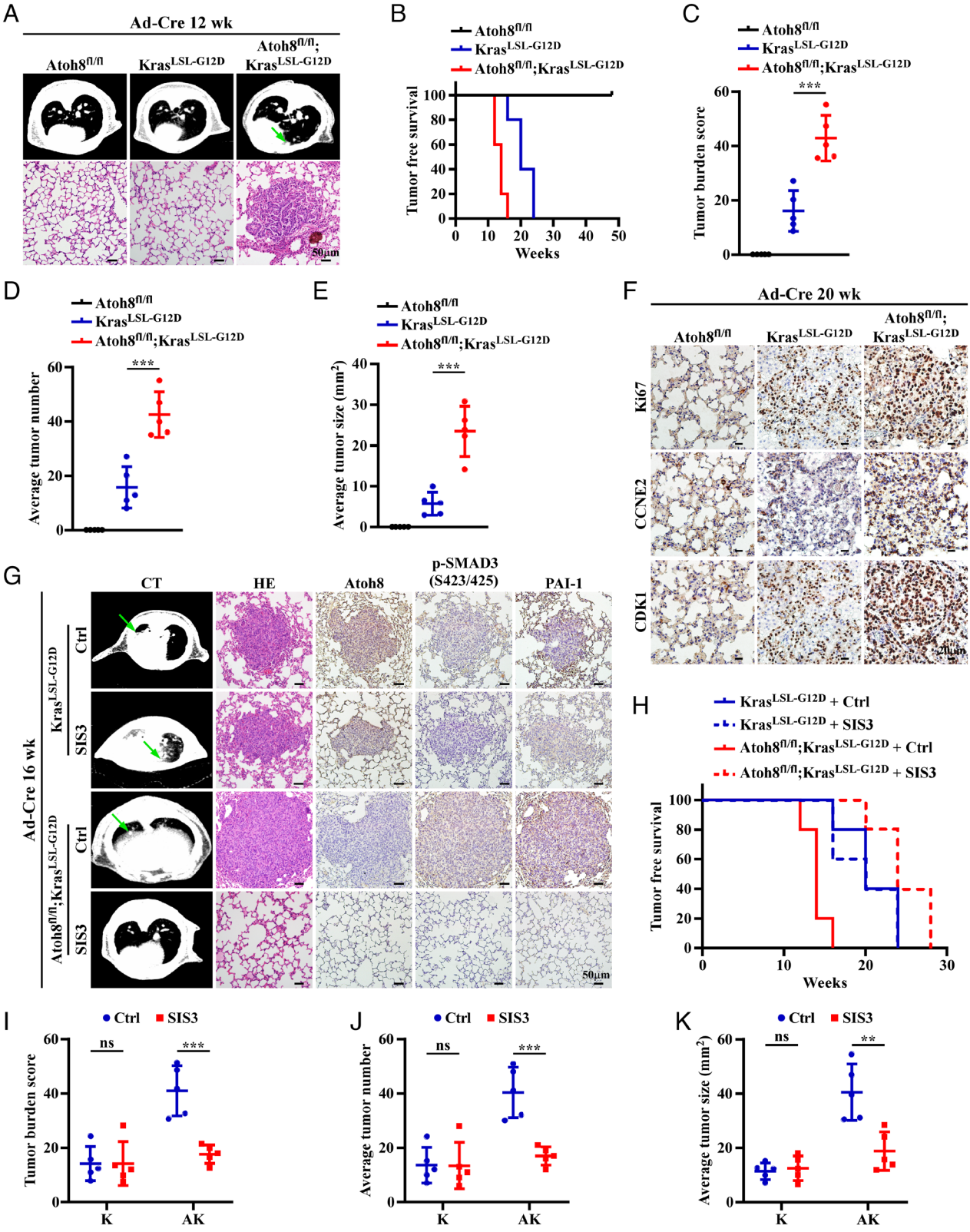

Fig. 5. Conditional deletion of Atoh8 accelerates Ras-driven lung tumorigenesis. (*A*) Representative images of micro-CT scanning and H&E of Atoh8$^{fl/fl}$Kras$^{LSL-G12D}$, and Atoh8$^{fl/fl}$;Kras$^{LSL-G12D}$ mice at 12 wk after Ad-Cre treatment. (*B*) Kaplan–Meier analysis of tumor-free survival of indicated mice (n = 5 each group) according to the micro-CT imaging and H&E staining. (*C–E*) Quantification of tumor burden score, average tumor number, and average tumor size at 24 wk after Ad-Cre treatment. (*F*) Representative images of Immunohistochemistry (IHC) staining for Ki67, ATOH8, CCNE2, and CDK1 in lung tissue at 20 wk after Ad-Cre treatment. (*G*) Representative images of micro-CT scanning and H&E and IHC staining of phosphorylated SMAD3, PAI-1, and Atoh8 at 16 wk after i.p. injection with control solvent or SMAD3 inhibitor SIS3 (5 mg/kg). (*H*) Tumor-free survival of indicated mice (n = 5 each group). (*I–K*) Quantification of tumor burden score, average tumor number, and average tumor size in indicated mice at 28 wk. Tumor Burden Score[2] (TBS) = (maximum tumor diameter)^2+ (number of tumors)^2. Two-tailed Student's *t* test was used for statistical analysis in *C*, *D*, *E*, *I*, *J*, and *K*. $^{**}P < 0.01$, $^{***}P < 0.001$, ns, not significant.

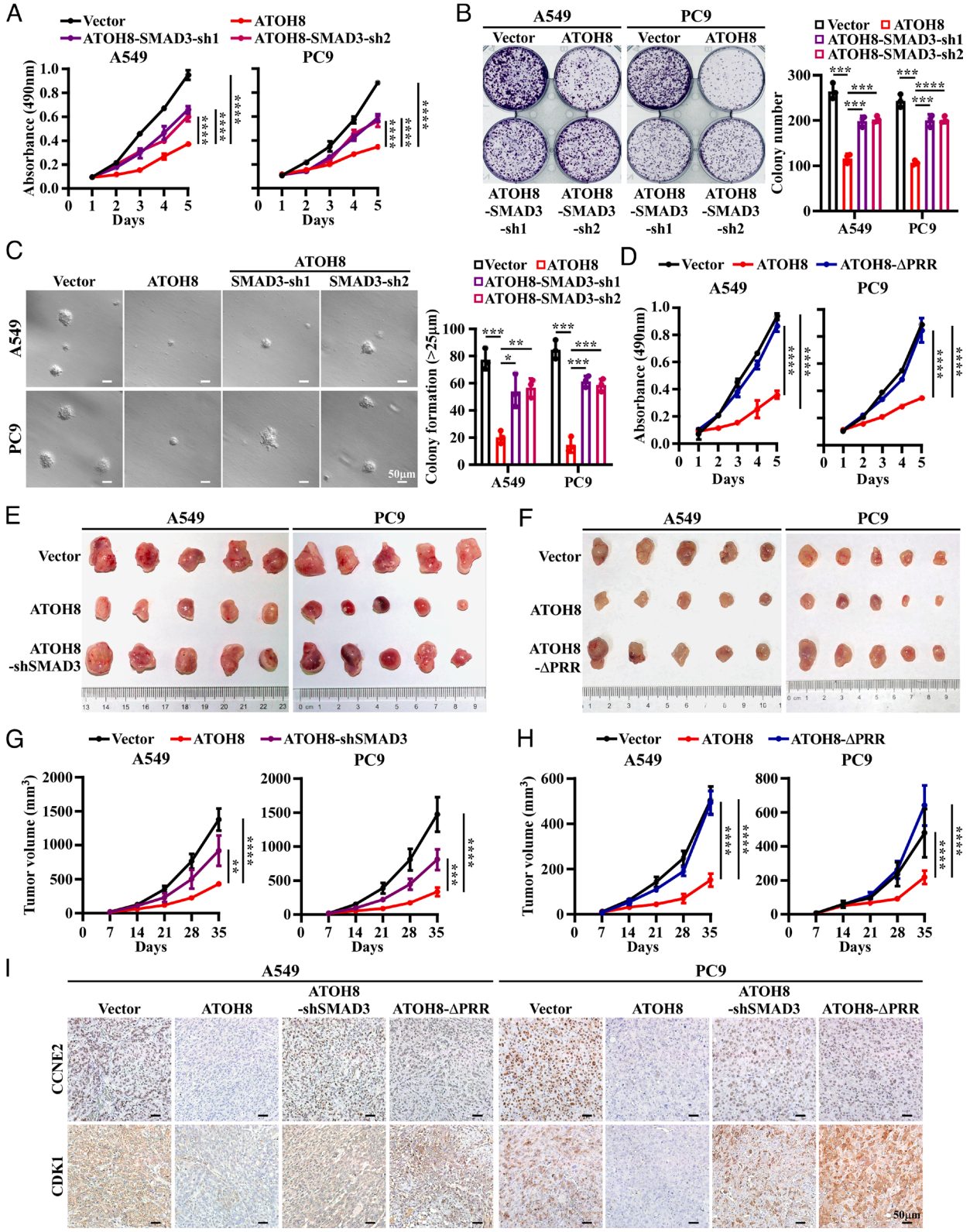

Fig. 6. SMAD3 is essential for the tumor-suppressive function of ATOH8. (*A–C*) The effects of SMAD3 silencing on cell growth at day 5 after stable cell establishment. (*D*) MTT assay of indicated cells. (*E–H*) Excised tumors and growth curves of the indicated tumor xenografts are shown. (*I*) Representative images of IHC staining of CCNE2 and CDK1. Error bars represent mean ± SD derived from three or four independent experiments. Two-tailed Student's *t* test was used for statistical analysis in *B* and *C*. Two-way ANOVA was used for statistical analysis in *A*, *D*, *G*, and *H*. **P* < 0.05, ***P* < 0.01, ****P* < 0.001, and *****P* < 0.0001.

significant negative correlation between expression of ATOH8 and CCNE2 and CDK1 (Fig. 3*L*). Moreover, overexpressing ATOH8 in lung cancer cells A549 (harboring wild-type TP53 and Rb genes but with low-level p53 expression probably due to methylation of TP53 gene and high-level MDM4 (28, 29) and PC9 (harboring gain-of-function mutant p53 (30), both of

which bear extremely low levels of endogenous ATOH8 because of high DNA methylation of the *ATOH8* gene, significantly decreased the percentages of G1/S cells and increased G2/M cell percentages, leading to cell proliferation inhibition, without altering the p53 and p16/Rb pathways (Fig. 3*M* and *SI Appendix*, Fig. S4 *C–F*). When released from the synchronized G1 phase, depleting ATOH8 in BEAS-2B cells accelerated G1/S and G2/M progression and promoted cell proliferation (Fig. 3*N* and *SI Appendix*, Fig. S4 *G* and *H*). In consistence, cell cycle genes promoting G1/S and G2/M transition were highly enriched in lung cancer tissues with low ATOH8 levels (*SI Appendix*, Fig. S4*I*). These results suggest that the ATOH8–SMAD3 complex can function as a transcriptional repressor to induce a cell cycle arrest signature.

Silencing ATOH8 Converts RIS into Malignant Transformation Requiring SMAD3. Lung epithelial cells presilenced for ATOH8 did not exhibit senescence phenotypes following oncogenic Ras overexpression, in which presilencing ATOH8 affected neither the canonical Ras signaling nor the p53, p15, or p16/Rb pathways (Fig. 4 *A* and *B* and *SI Appendix*, Fig. S5 *A* and *B*). Consistently, silencing ATOH8 potently abrogated oncogenic Ras-induced expression of numerous SASP molecules (*SI Appendix*, Fig. S5*C*). On the contrary, ATOH8 loss and activated Ras conferred BEAS-2B cells abilities to grow as cancerous cells (Fig. 4*C* and *SI Appendix*, Fig. S5*D*). Importantly, BEAS-2B cells silenced for ATOH8 and overexpressing oncogenic Ras formed subcutaneous tumor xenografts featured by adenocarcinoma histology in nude mice with 100% tumorigenic frequency, whereas vector control, senescent, or ATOH8-silenced BEAS-2B cells displayed no tumorigenicity without tumor growth curves (Fig. 4 *D–F* and *SI Appendix*, Fig. S5*E*). Moreover, silencing SMAD3 significantly compromised proliferative and tumorigenic abilities of the transformed BEAS-2B cells as induced by ATOH8 silencing and oncogenic Ras and, interestingly, reinduced expression of many SASP molecules (Fig. 4 *G* and *H* and *SI Appendix*, Fig. S5 *F* and *G*). Also notably, silencing ATOH8 hardly reversed the effects of mutant Ras on changing expression of Snail and E-cadherin, whereas further knocking down SMAD3 reversed their expression (*SI Appendix*, Fig. S5 *B* and *F*). Impressively, when SMAD3 was silenced, transformed BEAS-2B cells only formed one subcutaneous tumor xenograft with quite small tumor size when injected into five nude mice, and expression of Ki67, CCNE2, and CDK1 was dramatically decreased in this resultant tumor xenograft (Fig. 4 *I–K*). Although silencing SMAD3 abrogated RIS (Fig. 1 *I–K*), it failed to transform lung epithelial cells overexpressing oncogenic Ras. These data strongly demonstrate that silencing ATOH8 converts RIS into malignant transformation, relying on the oncogenic role of SMAD3.

Atoh8 Knockout Accelerates Ras-Driven Lung Tumorigenesis Requiring SMAD3. We further employed Atoh8$^{fl/fl}$, Kras$^{LSL-G12D}$, and Atoh8$^{fl/fl}$;Kras$^{LSL-G12D}$ mice to evaluate the effect of depleting Atoh8 on Ras-driven tumorigenesis. As shown in Fig. 5*A*, at about week 12 after Cre recombinase adenovirus treatment via nasal inhalation to induce Ras activation and/or homogeneous Atoh8 deletion in the lung tissue, neither the Atoh8$^{fl/fl}$ nor Kras$^{LSL-G12D}$ mice developed detectable lung tumors, whereas Atoh8$^{fl/fl}$;Kras$^{LSL-G12D}$ mice formed lung adenocarcinoma (LAD). The median time for LAD formation in Kras$^{LSL-G12D}$ mice was 20 wk, as compared with the time period of only 14 wk in Atoh8$^{fl/fl}$;Kras$^{LSL-G12D}$ mice, which bear increased tumor burden, tumor number, and tumor size (Fig. 5 *B–E*). Moreover, when collected at 20 wk, LAD tissue obtained from Atoh8$^{fl/fl}$;Kras$^{LSL-G12D}$ mice displayed a high proportion of Ki67-positive cancerous cells and high levels of CDK1 and CCNE2, which were markedly decreased in LAD tissue derived from Kras$^{LSL-G12D}$ mice and were almost absent in normal lung tissue of Atoh8$^{fl/fl}$ mice (Fig. 5*F*). Importantly, Atoh8$^{fl/fl}$;Kras$^{LSL-G12D}$ mice, but not Kras$^{LSL-G12D}$ mice, intraperitoneally injected with a specific SMAD3 inhibitor SIS3, which indeed decreased SMAD3 phosphorylation and PAI-1 expression, needed more than 20 wk to form LAD with alleviated tumor burden, tumor number, and tumor size (Fig. 5 *G–K*). It is noteworthy that a mild downregulation of ATOH8 levels in the Kras-only tumor tissues was detected (Fig. 5*G*), which might facilitate Kras-driven tumorigenesis. These data strongly suggest that conditional deletion of Atoh8 in the lung tissue potently accelerates oncogenic Ras-driven lung tumorigenesis in a fashion requiring SMAD3 and that targeting SMAD3 specifically exerts therapeutic effects against lung cancer bearing both mutant Ras and ATOH8 loss.

ATOH8–SMAD3 Complex Achieves Potent Tumor-Suppressive Effects. Notably, overexpression of full-length ATOH8 but not ATOH8 deleted for the bHLH (ATOH8-ΔbHLH) domain, which is essential for DNA binding, potently inhibited, whereas silencing ATOH8 accelerated cell growth, and tumor formation, without affecting the Ras/MEK/ERK signaling (*SI Appendix*, Fig. S6 *A–K*). Of note, silencing SMAD3 markedly attenuated the TGF-β signaling activity and promoted cell and tumor growth of ATOH8-overexpressing lung cancer cells; overexpressing ATOH8-ΔPRR, which is unable to bind SMAD3, failed to suppress cell and tumor growth (Fig. 6 *A–H* and *SI Appendix*, Fig. S7 *A–D*). In these resultant tumor xenografts, the inhibitory effects of ATOH8 overexpression on the percentages of Ki67-positive cells and expression levels of CCNE2 and CDK1 could be reversed by silencing SMAD3 (Fig. 6*I* and *SI Appendix*, Fig. S7*E*), suggesting that SMAD3 is indeed essential for the tumor-suppressive effects of ATOH8.

ATOH8 Gene Is Hypermethylated and Clinically Significant in Human Non-Small Cell Lung Cancer (NSCLC). ATOH8 was significantly down-regulated in NSCLC tissue and low-level ATOH8 correlated with shorter median overall survival (OS), especially in stage I patients (Fig. 7 *A* and *B* and *SI Appendix*, Fig. S8 *A* and *B*). ATOH8 protein levels were also down-regulated in eight cases of NSCLC tissue, and ATOH8 was weakly immunostained in 143 Lung Adenocarcinoma (LUAD) and almost undetectable in 45 Lung Squamous Cell Carcinoma (LUSC) tissue specimens (Fig. 7*C* and *SI Appendix*, Fig. S8 *C* and *D*). A total of 101 LUAD patients bearing low ATOH8 proteins exhibited 98-mo median OS, whereas 42 ATOH8-high LUAD patients survived for over 140-mo median OS (Fig. 7*D*). Moreover, the proportion of high-level phosphorylated SMAD3 was higher in NSCLC tissues bearing low ATOH8 expression as compared with those with relatively high ATOH8 expression (Fig. 7 *E* and *F*), indicating that SMAD3 can be an active tumor promoter in ATOH8-absent lung cancer. Notably, genetic alternations in ATOH8 gene loci are rare (*SI Appendix*, Fig. S8*E*). Instead, a large CpG island with approximately 1,699-bp length spanned across the ATOH8 gene loci (Fig. 7*G*). The average value of the highest quantile of β-value that defines the methylation level of ATOH8 gene was 0.21 in lung tumors, which was only 0.07 in normal lung tissue (Fig. 7*H*). In contrast to a well-known tumor suppressor CDKN2A (31), whose methylation was only 0.66% in 463 LUAD specimens, high

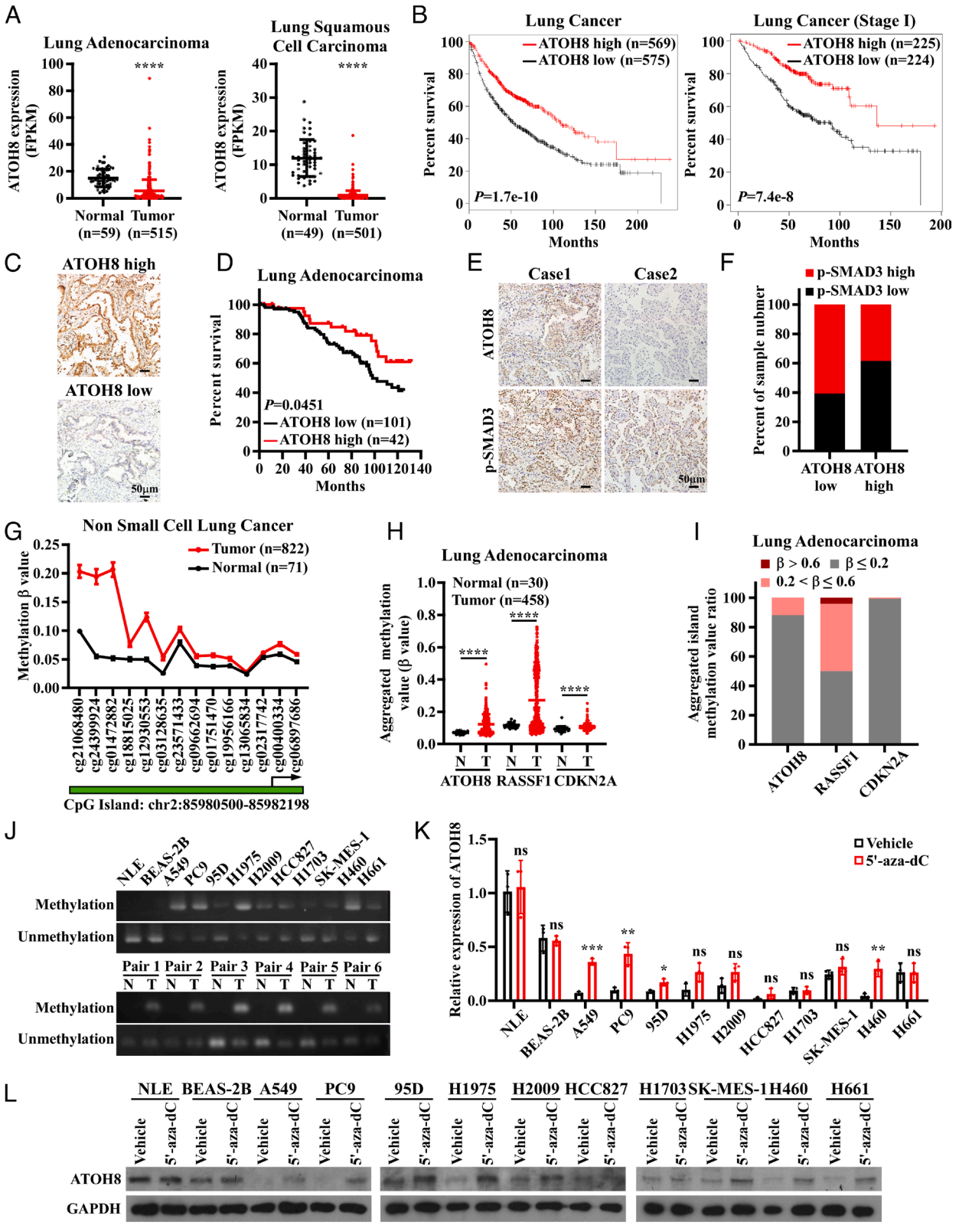

Fig. 7. ATOH8 is down-regulated by hypermethylation and has clinical significance. (*A* and *B*) Expression profile of ATOH8 and OS of NSCLC patients in the TCGA LUAD and LUSC datasets. (*C* and *D*) Representative images of ATOH8 immunostaining in 143 LUAD specimens collected by this study and their OS analysis. (*E*) Representative images of IHC staining of phosphorylated SMAD3 and ATOH8 in NSCLC tissues. (*F*) The correlation between levels of phosphorylated SMAD3 and ATOH8 in 41 NSCLC patients. (*G*) The methylation level of ATOH8 in lung tumor (n = 822) and normal lung tissues (n = 71) from the TCGA methylation database using SMART web tool. (*H*) Aggregated methylation values of ATOH8, RASSF1, and CDKN2A in LUAD (n = 458) and normal lung tissues (n = 30) from the TCGA methylation database. (*I*) The proportion of 458 LUAD patients according to the β-values of methylation levels of indicated genes. (*J*) Methylation-specific PCR measured the methylation status of ATOH8. (*K* and *L*) The effect of 5-aza-dC (1 μM) treatment for 72 h on ATOH8 expression. Error bars represent mean ± SD derived from three independent experiments. Two-tailed Student's *t* test was used for statistical analysis in *A*, *H*, and *K*. *$P < 0.05$, **$P < 0.01$, ***$P < 0.001$, ****$P < 0.0001$, ns, not significant.

levels of ATOH8 gene methylation were found in 11.8% of these specimens (Fig. 7*I*) similar to a hypermethylated gene RASSF1 in lung cancer (32). The methylation level of ATOH8 negatively correlated with its expression (*SI Appendix*, Fig. S8*F*). Moreover, the ATOH8 gene methylation was detectable in six cases of NSCLC tissues and a series of NSCLC cell lines but not in any paired normal lung tissue or lung epithelial cells (Fig. 7*J*). When treated with 5-aza-2′-deoxycytidine, a DNA methyltransferase inhibitor, NSCLC cell lines harboring ATOH8 gene methylation displayed increased ATOH8 expression (Fig. 7 *K* and *L*). These results support the notion that ATOH8 as a tumor suppressor can be silenced by DNA methylation.

Discussion

OIS is an important barrier against malignant transformation and is generally governed by tumor suppressors, such as p53 and p16 (6). However, p53- and p16-dependent cellular senescence was mostly found in mesenchymal cells, such as fibroblasts, and Ras or B-RAF proto-oncogene (BRAF) can cause senescence in p53- or p16-deficient human fibroblasts or melanocytes (33–35). Malignant transformation occurs commonly when oncogene is activated together with inactivation of tumor suppressor. The biological process underlying the conversion between cellular senescence and malignant transformation is poorly understood. This study describes a scenario that in NLE cells harboring either intact or impaired p53 and p16/Rb pathways, oncogenic Ras could still induce cellular senescence independent of the p53 and p16/Rb pathways. TGF-β1 instead is abundantly induced to overactivate SMAD3, which formed a transcriptional complex with ATOH8 to repress a series of cell cycle–promoting genes, leading to a cellular senescence phenotype. When Ras overactivation occurs in ATOH8-lost cells, cellular senescence can be overcome and converted to malignant transformation in a SMAD3-dependent manner. Consistently, in lung cancer cells harboring wild-type or aberrant p53 and p16/Rb pathways, ATOH8 exerts potent tumor-suppressive roles that require SMAD3, without altering p53 or p16/Rb pathways. These findings not only demonstrate how a crucial SASP-derived cytokine initiates epithelial cellular senescence directed by a potential tumor suppressor–controlled transcriptional program but also suggest that ATOH8 loss and Ras mutation may represent a two-hit scenario for tumorigenesis.

SASP can exhibit both tumor-suppressive and tumor-promoting effects during cancer initiation and development (7, 36). TGF-β, a key component of the SASP, functions as an early tumor repressor and late tumor promoter (8, 17). Previous studies on the tumor-suppressive and transforming effects of TGF-β were extensively investigated especially in SMAD4-mutant cancers, such as PDA and colon cancer (21–23, 37). However, the process of the conversion from cellular senescence and malignant transformation under TGF-β operation is poorly understood. Our current study deciphers that in lung epithelial cells high-level TGF-β1 stimulates formation of a tumor-suppressive transcriptional complex SMAD3–ATOH8 to induce OIS, whereas it is switched to promote malignant transformation when the SMAD3–ATOH8 complex is disrupted due to ATOH8 loss, which potently accelerates tumorigenesis of lung cancer that usully bears intact TGF-β signaling components. Therefore, whether TGF-β1 induces cellular senescence or transformation relies on a tumor suppressor–governed anti–cell cycle program, suggesting that TGF-β1 can function as not only an early tumor suppressor but also a promoter of transformation.

The complexity of TGF-β signaling is fueled by the notion that SMAD proteins can direct quite different transcriptional responses (38, 39). However, how they determine the prosenescent versus transforming effects of TGF-β is poorly investigated. In keratinocytes, deletion of SMAD3, but not SMAD2 or SMAD4, delays mutant Ras–induced senescence, overexpressing SMAD3 directly induces senescence, and SMAD3 null converts benign papilloma formed by Ras-mutant keratinocytes to malignant carcinoma (40), suggesting a consistent tumor-suppressive role of SMAD3. However, SMAD3 can play important oncogenic roles even in skin cancer (41, 42). Our study characterizes SMAD3 as a determinant deciding TGF-β–mediated cellular response during oncogenesis, which is not only essential for oncogenic Ras-driven senescence but also important for malignant transformation, and provides an explanation for the long-lasting puzzle that how SMAD3 switches from a tumor suppressor to a tumor promoter. Notably, SMAD proteins normally bind with low affinity to DNA and require other transcription cofactors to achieve high DNA-binding affinity (43). In such a context, this study identifies the ATOH8–SMAD3 transcriptional complex, which represses a series of cell cycle–promoting genes through binding distinct consensus motifs, indicating a noncanonical TGF-β/SMAD3 pathway. Additionally, unlike SMAD4 and SMAD2, SMAD3 is rarely mutated in human cancers (44). Our study suggests that loss of ATOH8 leading to disruption of the ATOH8–SMAD3 complex and switch of tumor-suppressive SMAD3 to be oncogenic might be the key mechanism underlying TGF-β signaling-mediated tumor initiation.

Of interest, our study identifies a potential noncanonical tumor suppressor ATOH8 without significant genetic mutations. Instead, ATOH8 gene methylation can be found in 11.8% of LUAD tissue comparable to two hypermethylated genes, namely, CDKN2A and RASSF1 (31, 32). This suggests that ATOH8 hypermethylation is a frequent event, especially in LUAD. Because of the lack of early detection biomarkers, more than two thirds of them were initially diagnosed with advanced diseases. Since abnormal DNA methylation can occur during the onset of tumor initiation and can be detected in body fluid specimens (45, 46), ATOH8 gene methylation–based liquid biopsy might represent a strong candidate as early detection and diagnostic biomarker for lung cancer. Notably, although clinical drug targeting specific Ras mutation (Ras^{G12C}) is promising, therapeutic strategies targeting Ras-mutant cancers are far from being clinically applicable. This study demonstrates that spontaneous lung tumor formation in mouse models driven by mutant Ras and Atoh8 depletion, but not by mutant Ras alone, can be significantly delayed by a SMAD3 inhibitor, suggesting that detecting ATOH8 gene methylation might represent an indicator for use of SMAD-targeted treatments for Ras-mutant NSCLC patients.

Methods

Lung cancer clinical samples and information were collected from the Sun Yat-sen University Cancer Center. All animal experiments were approved by the Sun Yat-sen University Institutional Animal Care and Use Committee. Details of materials regarding cell lines, plasmids, human tissue specimens, antibodies, and reagents used in this study are provided in *SI Appendix*. Detailed methods of cell culture, plasmid transfection, RNA extraction, and real-time PCR, IP, SPR, IF, PLA, WB, IHC, EMSA, ChIP, clonogenic assay and soft agar colony formation assay, cell cycle analysis, mouse models and treatments, and data analysis can also be found in *SI Appendix*.

Data, Materials, and Software Availability. RNA seq and ChIP seq data have been deposited in Gene Expression Omnibus (GSE190062).

ACKNOWLEDGMENTS. This work was supported by the Key Program of the National Natural Science Foundation of China (82030088, 81820108025, 82241231); the Natural Science Foundation of China (81922050, 81972170); The Foundation for Innovative Research Groups of the National Natural Science Foundation of China (81621004); the Open Project of State Key Laboratory of Respiratory Disease (SKLRD-OP-202201, SKLRD-OP-202316).

Author affiliations: [a]Department of Immunology, Sun Yat-sen University Zhongshan School of Medicine, Guangzhou 510080, China; [b]Cancer Institute, Southern Medical University, Guangzhou 510515, China; [c]State Key Laboratory of Respiratory Diseases and Guangzhou Institute of Respiratory Diseases, The First Affiliated Hospital of Guangzhou Medical University, Guangzhou 510120, China; [d]Department of Pathology, Collaborative Innovation Center for Cancer Medicine, State Key Laboratory of Oncology in South China, Sun Yat-sen University Cancer Center, Guangzhou 510060, China; [e]Department of General Internal Medicine, State Key Laboratory of Oncology in South China, Sun Yat-sen University Cancer Center, Guangzhou 510060, China; [f]Department of Molecular Oncology, H. Lee Moffitt Cancer Center and Research Institute, Tampa 33612, FL; and [g]Guangdong Engineering and Technology Research Center for Disease-Model Animals, Sun Yat-sen University, Guangzhou 510006, China

1. S. Li, A. Balmain, C. M. Counter, A model for RAS mutation patterns in cancers: Finding the sweet spot. *Nat. Rev. Cancer* **18**, 767–777 (2018).
2. L. Johnson *et al.*, Somatic activation of the K-ras oncogene causes early onset lung cancer in mice. *Nature* **410**, 1111–1116 (2001).
3. M. Serrano, A. W. Lin, M. E. McCurrach, D. Beach, S. W. Lowe, Oncogenic ras provokes premature cell senescence associated with accumulation of p53 and p16INK4a. *Cell* **88**, 593–602 (1997).
4. A. G. Stephen, D. Esposito, R. K. Bagni, F. McCormick, Dragging ras back in the ring. *Cancer Cell* **25**, 272–281 (2014).
5. A. Hernandez-Segura, J. Nehme, M. Demaria, Hallmarks of cellular senescence. *Trends Cell Biol.* **28**, 436–453 (2018).
6. D. Munoz-Espin, M. Serrano, Cellular senescence: From physiology to pathology. *Nat. Rev. Mol. Cell Biol.* **15**, 482–496 (2014).
7. J. P. Coppe, P. Y. Desprez, A. Krtolica, J. Campisi, The senescence-associated secretory phenotype: The dark side of tumor suppression. *Annu. Rev. Pathol.* **5**, 99–118 (2010).
8. Y. Zhang, P. B. Alexander, X. F. Wang, TGF-beta family signaling in the control of cell proliferation and survival. *Cold Spring Harb. Perspect. Biol.* **9**, a022145 (2017).
9. K. Tominaga, H. I. Suzuki, TGF-beta signaling in cellular senescence and aging-related pathology. *Int. J. Mol. Sci.* **20**, 5002 (2019).
10. L. Cassar *et al.*, TGF-beta receptor mediated telomerase inhibition, telomere shortening and breast cancer cell senescence. *Protein Cell* **8**, 39–54 (2017).
11. S. Senturk *et al.*, Transforming growth factor-beta induces senescence in hepatocellular carcinoma cells and inhibits tumor growth. *Hepatology* **52**, 966–974 (2010).
12. A. R. Nobre *et al.*, Bone marrow NG2(+)/Nestin(+) mesenchymal stem cells drive DTC dormancy via TGFbeta2. *Nat. Cancer* **2**, 327–339 (2021).
13. F. Debacq-Chainiaux *et al.*, Repeated exposure of human skin fibroblasts to UVB at subcytotoxic level triggers premature senescence through the TGF-beta1 signaling pathway. *J. Cell Sci.* **118**, 743–758 (2005).
14. G. Lyu *et al.*, TGF-beta signaling alters H4K20me3 status via miR-29 and contributes to cellular senescence and cardiac aging. *Nat. Commun.* **9**, 2560 (2018).
15. J. C. Acosta *et al.*, A complex secretory program orchestrated by the inflammasome controls paracrine senescence. *Nat. Cell Biol.* **15**, 978–990 (2013).
16. M. Reimann *et al.*, Tumor stroma-derived TGF-beta limits myc-driven lymphomagenesis via Suv39h1-dependent senescence. *Cancer Cell* **17**, 262–272 (2010).
17. J. Massague, TGFbeta in cancer. *Cell* **134**, 215–230 (2008).
18. M. J. Macias, P. Martin-Malpartida, J. Massague, Structural determinants of Smad function in TGF-beta signaling. *Trends Biochem. Sci.* **40**, 296–308 (2015).
19. J. Seoane, H. V. Le, L. Shen, S. A. Anderson, J. Massague, Integration of Smad and forkhead pathways in the control of neuroepithelial and glioblastoma cell proliferation. *Cell* **117**, 211–223 (2004).
20. Z. Ying *et al.*, CCT6A suppresses SMAD2 and promotes prometastatic TGF-beta signaling. *J. Clin. Invest.* **127**, 1725–1740 (2017).
21. C. J. David *et al.*, TGF-beta tumor suppression through a lethal EMT. *Cell* **164**, 1015–1030 (2016).
22. Y. H. Huang *et al.*, ID1 mediates escape from TGFbeta tumor suppression in pancreatic cancer. *Cancer Discov.* **10**, 142–157 (2020).
23. J. Su *et al.*, TGF-beta orchestrates fibrogenic and developmental EMTs via the RAS effector RREB1. *Nature* **577**, 566–571 (2020).
24. H. J. Faust *et al.*, IL-17 and immunologically induced senescence regulate response to injury in osteoarthritis. *J. Clin. Invest.* **130**, 5493–5507 (2020).
25. Z. Novakova *et al.*, Cytokine expression and signaling in drug-induced cellular senescence. *Oncogene* **29**, 273–284 (2010).
26. C. N. Nagineni *et al.*, Radiation-induced senescence reprograms secretory and metabolic pathways in colon cancer HCT-116 cells. *Int. J. Mol. Sci.* **22**, 4835 (2021).
27. L. Golomb *et al.*, Age-associated inflammation connects RAS-induced senescence to stem cell dysfunction and epidermal malignancy. *Cell Death Differ.* **22**, 1764–1774 (2015).
28. S. Kouidou *et al.*, Non-CpG cytosine methylation of p53 exon 5 in non-small cell lung carcinoma. *Lung Cancer* **50**, 299–307 (2005).
29. S. Tornaletti, G. P. Pfeifer, Complete and tissue-independent methylation of CpG sites in the p53 gene: Implications for mutations in human cancers. *Oncogene* **10**, 1493–1499 (1995).
30. M. Pan *et al.*, TP53 gain-of-function and non-gain-of-function mutations are differentially associated with sidedness-dependent prognosis in metastatic colorectal cancer. *J. Clin. Oncol.* **40**, 171–179 (2022).
31. R. Zhao, B. Y. Choi, M. H. Lee, A. M. Bode, Z. Dong, Implications of genetic and epigenetic alterations of CDKN2A (p16(INK4a)) in cancer. *EBioMedicine* **8**, 30–39 (2016).
32. J. Li *et al.*, RASSF1A promoter methylation and Kras2 mutations in non small cell lung cancer. *Neoplasia* **5**, 362–366 (2003).
33. W. Wei, R. M. Hemmer, J. M. Sedivy, Role of p14(ARF) in replicative and induced senescence of human fibroblasts. *Mol. Cell Biol.* **21**, 6748–6757 (2001).
34. S. Haferkamp *et al.*, Oncogene-induced senescence does not require the p16(INK4a) or p14ARF melanoma tumor suppressors. *J. Invest. Dermatol.* **129**, 1983–1991 (2009).
35. C. Michaloglou *et al.*, BRAFE600-associated senescence-like cell cycle arrest of human naevi. *Nature* **436**, 720–724 (2005).
36. J. Birch, J. Gil, Senescence and the SASP: Many therapeutic avenues. *Genes Dev.* **34**, 1565–1576 (2020).
37. B. Zhang *et al.*, Antimetastatic role of Smad4 signaling in colorectal cancer. *Gastroenterology* **138**, e961–e963 (2010).
38. N. R. Gough, X. Xiang, L. Mishra, TGF-beta signaling in liver, pancreas, and gastrointestinal diseases and cancer. *Gastroenterology* **161**, 434–452.e15 (2021).
39. C. J. David, J. Massague, Contextual determinants of TGFbeta action in development, immunity and cancer. *Nat. Rev. Mol. Cell Biol.* **19**, 419–435 (2018).
40. K. Vijayachandra, J. Lee, A. B. Glick, Smad3 regulates senescence and malignant conversion in a mouse multistage skin carcinogenesis model. *Cancer Res.* **63**, 3447–3452 (2003).
41. A. G. Li, S. L. Lu, M. X. Zhang, C. Deng, X. J. Wang, Smad3 knockout mice exhibit a resistance to skin chemical carcinogenesis. *Cancer Res.* **64**, 7836–7845 (2004).
42. S. H. Tannehill-Gregg, D. F. Kusewitt, T. J. Rosol, M. Weinstein, The roles of Smad2 and Smad3 in the development of chemically induced skin tumors in mice. *Vet Pathol.* **41**, 278–282 (2004).
43. Y. Shi *et al.*, Crystal structure of a Smad MH1 domain bound to DNA: Insights on DNA binding in TGF-beta signaling. *Cell* **94**, 585–594 (1998).
44. J. Seoane, R. R. Gomis, TGF-beta family signaling in tumor suppression and cancer progression. *Cold Spring Harb. Perspect Biol.* **9**, a022277 (2017).
45. A. Koch *et al.*, Analysis of DNA methylation in cancer: Location revisited. *Nat. Rev. Clin. Oncol.* **15**, 459–466 (2018).
46. H. Kim *et al.*, Tumor-specific methylation in bronchial lavage for the early detection of non-small-cell lung cancer. *J. Clin. Oncol.* **22**, 2363–2370 (2004).